Cavity-Shape-Dependent Divergent Chemical Reaction inside Aqueous Pd_6L_4 Cages

Debsena Chakraborty, Shamsad Ali, Pritam Choudhury, Neal Hickey, and Partha Sarathi Mukherjee*

ABSTRACT: Chemical reactions inside the confined pockets of enzyme-mimicking hosts, such as cages and macrocycles, have been an emerging field of interest over the past decade. Although many such reactions are known, the use of such cages toward the divergent synthesis of nonisomeric products has not been well explored. Divergent synthesis is a technique of forming two or more distinct products from the same reagents by changing the catalyst or reaction conditions. Changing the shape of the cage can also change the nature and magnitude of the host–guest interactions. Thus, is it possible for such changes to cause differences in the reaction pathways leading to formation of nonisomeric products? Herein, we report a divergent chemical transformation of anthrone [anthracen-9(10*H*)-one] inside different water-soluble M_6L_4 cages. When anthrone was encapsulated inside a newly synthesized M_6L_4 octahedral cage **1**, it dimerized to form dianthrone [9,9′-bianthracen-10,10′(9*H*,9′*H*)-dione]. In contrast, when the same chemical reaction was performed inside a M_6L_4 double-square shaped cage **2**, it was oxidized to form anthraquinone [anthracene-9,10-dione]. Similar results were obtained with a different set of isomeric aqueous Pd_6 cages **3a** (octahedral cage) and **3b** (double-square cage), indicating the dependence of the shape of cavity on the divergent synthesis. The present report demonstrates a unique example of different outcomes/results of a reaction depending on the shape of the molecular container, which was driven by the host–guest interactions and the preorganization of the substrates.

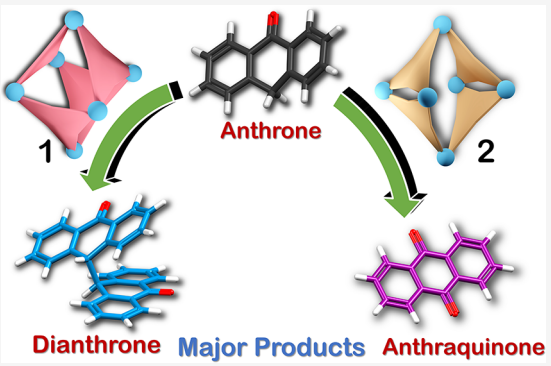

1. INTRODUCTION

In nature, many reactions occur in the confined spaces of biomolecules, such as enzymes and other cell organelles. Such reactions are known to show an enhanced reaction rate and selectivity.[1] Multiple noncovalent interactions, such as ion–pair interactions, hydrogen bonding, electronic polarization, $\pi-\pi$ interactions, and van der Waals interactions, are responsible for this enhanced rate and selectivity.[2] Inspired by such biomolecules, scientists have developed various artificial analogues that mimic the different properties of such molecules. These artificial analogues are either "polymeric" like metal organic frameworks (MOFs) and covalent organic frameworks (COFs) or "discrete" like cages and macrocycles.[3−8] Discrete hosts have better solubility and have been used for different biomimetic applications.[9] Discrete hosts can be either organic or metal–organic. Organic cages or macrocycles are generally neutral and soluble in common organic solvents. For this reason, most organic cages[10−13] and macrocycles do not bind strongly to soluble organic guests, and instances of guest uptake and subsequent chemical transformation inside the cavity are less explored.[14] Metal–organic cages, on the other hand, are charged. Their solubility depends on the counterion used, and they can be dissolved in polar solvents like water.[15,16] Such hosts are often formed through the self-assembly of metal acceptor and donor subunits, forming the thermodynamically most stable system. Through this metal–ligand-coordination-driven self-assembly, thermodynamically stable products can be easily obtained without the need of multistep synthesis processes. This makes metal–ligand self-assembly a valuable tool for the synthesis of different hosts of varying structural complexity.[17,18] Specifically, these water-soluble hosts are highly sought after due to their amenability to biological environments and efficient guest encapsulation capability. Such a capability is due to a combination of hydrophobic interactions between the host and guest, which causes tight binding of the guest molecules inside the cage. All these aspects together make metal–organic hosts conducive for multiple applications such as sensing,[19,20] stabilization of reactive intermediates,[21,22] separation of molecules,[23,24] and platforms for light harvesting.[25−27]

Metal–organic cages have also been used as hosts for carrying out different organic reactions.[28,29] The reactions investigated include the Diels–Alder reaction,[30] the Knoevenagel condensation,[31] the Nazarov cyclization,[32] the aza-

Darzens Reaction,[33] oxidation reactions[34−38] and many more.[39−42] However, although quite a few reactions inside metal−organic hosts are known, many of them face multiple complications, like product inhibition and cage degradation by the products.[43] Probably for these reasons, most reactions inside cages are single-step; and multiple-step, cascade, or domino reactions are rare.[44,45] Similarly, cage dependent divergent reactions, other than regioselective ones,[30,46] are also unexplored inside cages.

Divergent reactions or divergent synthesis is defined as a reaction strategy where nonidentical products are formed from the same reactants by changing the reaction conditions or catalyst.[47] Divergent synthesis can be of various types, such as regio-divergent and diastereo-divergent synthesis, but the rarest of them are the divergent syntheses, where nonisomeric products are formed.[48] Such reactions are known predominately with organometallic or organic catalysts, where a change in catalyst changes the product obtained.[49] In such cases, one catalyst selectively stabilizes the transition state for one reaction, while a different catalyst stabilizes the transition state for a different reaction. In doing so, the catalyst dictates the flow of the reaction, and different products are formed.

In the case of reactions taking place inside the cavity of a cage, the stabilization comes from the noncovalent forces between the host and guest. The cumulative effect of such interactions can cause changes in the properties of the guest molecules from those observed in the bulk solvent.[50] Such interactions are also known to stabilize the transition state of the reactions occurring inside the cavity, which leads to an enhanced reaction rate.[51] These host−guest interactions depend on the host's nature, size, and shape. Thus, by changing the shape of the cavities, different transition states could be selectively stabilized, thereby leading to a divergent synthesis. However, to the best of our knowledge, no such example is known where changing the Pd(II) cage cavity has led to different reaction pathways and has led to the formation of distinct, nonisomeric products.

Herein, we report the synthesis of a water-soluble cage **1**, which was formed by the metal−ligand-coordination-driven self-assembly of a pyrimidine-based tripyridyl ligand **L1** with a 90° *cis*-blocked Pd^{II} acceptor **M** (Scheme 1). The crystal structure of **1** showed that it has an octahedral structure with a large cavity suitable for guest encapsulation. **1** was able to encapsulate a variety of planar and nonplanar molecules. Further, inside the cavity of cage **1**, anthrone (**AO**) [anthracen-9(10*H*)-one] readily dimerized to form dianthrone (**P1**) [9,9′-bianthracen-10,10′(9*H*,9′*H*)-dione]. This reaction was then performed inside a different cage (**2**),[31] which has the same stoichiometry (M_6L_4) but a different shape (double-square) with D_{2h}-symmetry (Scheme 1). Surprisingly, inside the cavity of cage **2**, **AO** underwent facile oxidation to form anthraquinone (**P2**) [anthracene-9,10-dione] instead of dimerizing to form **P1**. Further investigations revealed that the reaction inside the cages proceeded in such a way that the most stable host−guest complex was formed. This was achieved through preorganization of the substrates inside the cages. Inside cage **1**, **AO** molecules were preorganized in such a way that the formation of **P1** was facile and thus led to the formation of **P1**⊂**1**, which was a more stable host−guest complex. Similarly, in cage **2**, encapsulated **AO** proceeded to form **P2**, leading to the more stable host−guest species (**P2**⊂**2**) species. To the best of our knowledge, a similar dichotomy in the reaction pathway by changing the cavity shape of the reaction vessel has not yet been demonstrated.

Scheme 1. Schematic Representation of Divergent Synthesis Using Pd_6 Cages 1 and 2 of Different Shapes

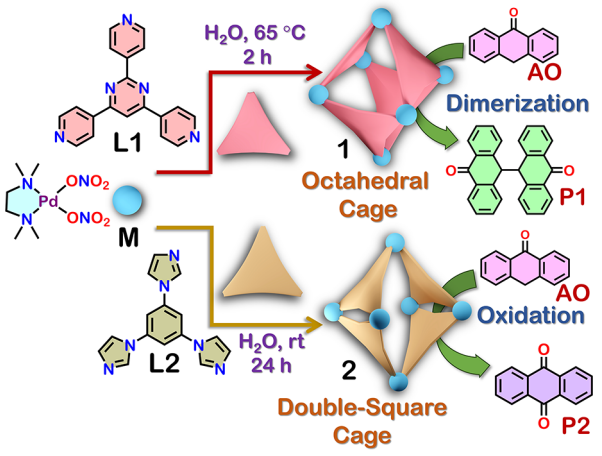

2. RESULTS AND DISCUSSION

2.1. Synthesis and Characterization. The tripyridyl ligand **L1** with a pyrimidine core was synthesized by the base-mediated condensation of 4-acetylpyridine and 4-pyridinecarbonitrile at 120 °C in an autoclave reactor (Scheme S1). The ligand was characterized by electrospray ionization mass spectrometry (ESI-MS), proton nuclear magnetic resonance (^{1}HNMR) and (carbon NMR)^{13}C NMR in $CDCl_3$ (Figures S1 and S2). Due to the unsymmetrical nature of the ligand **L1**, it had 2:1 splitting of the *α*- and *β*-hydrogen of the pyridine rings (Figures 1 and S1). These signals are denoted as *a* and *a*′ for the *α*-hydrogens of the pyridine rings and *b* and *b*′ for the *β*-hydrogens of the pyridine rings.

1 was synthesized by the self-assembly of **L1** with *cis*-[(tmeda)Pd(NO_3)$_2$] (**M**) [tmeda = *N*,*N*,*N*′,*N*′-tetramethylethane-1,2-diamine] in a 2:3 molar ratio in water at 65 °C for 2 h (Scheme S2). The mixture turned into a clear solution over

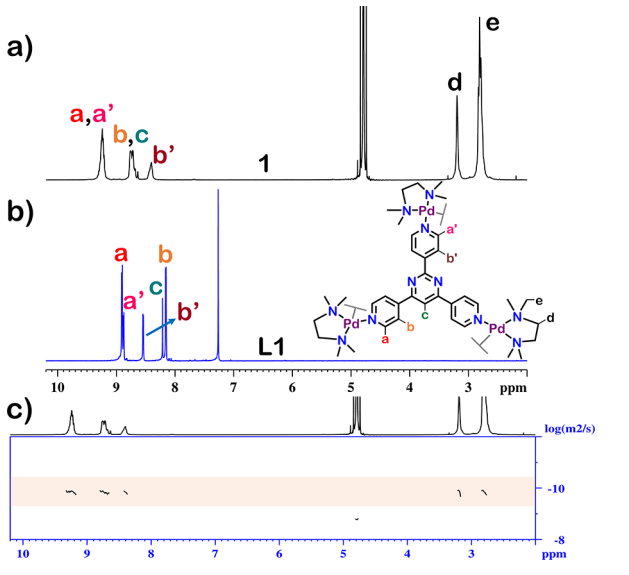

Figure 1. Stacked ^{1}H NMR spectra of (a) cage **1** in D_2O, (b) ligand **L1** in $CDCl_3$, and (c) ^{1}H NMR DOSY spectrum of **1** in D_2O.

the course of the reaction with the consumption of the donor. After the reaction was complete, the pure form of **1** was obtained by concentrating the solution under reduced pressure and triturating with acetone.

The nature of the product (**1**) formed was first characterized with ^{1}H NMR (in D_2O), which revealed three distinct peaks in the aromatic region (Figures 1 and S3). ^{1}H diffusion-ordered spectroscopy (DOSY) showed that all the three peaks correspond to the same assembly having a common diffusion band [$D = 1.58 \times 10^{-10}$ m^2 s^{-1} (log $D = -9.8$)] (Figures 1 and S4). The peaks were further characterized by ^{1}H−^{1}H correlation spectroscopy (COSY) and nuclear Overhauser enhancement spectroscopy (NOESY) NMR in D_2O (Figures S5 and S6). The analysis showed that the split α-hydrogen peaks (a and a′) of the pyridine rings in the ^{1}H NMR of **L1** were merged upon complexation with **M** in the ^{1}H NMR of **1**. Similarly, one of the β-hydrogen peaks (denoted as b) merged with the pyrimidine peak (denoted as c). This was also in line with the proton integration of **1** (Figure S3).

To understand the stoichiometry of the cage, the ESI-MS spectrum of the PF_6^- analogue was recorded in acetonitrile. The spectrum showed peaks at m/z = 719.0805, 935.5879, 1295.1059, and 2015.1970 corresponding to the fragments $[\mathbf{M_6L1_4}\ (PF_6)_7]^{5+}$, $[\mathbf{M_6L1_4}\ (PF_6)_8]^{4+}$, $[\mathbf{M_6L1_4}\ (PF_6)_9]^{3+}$, and $[\mathbf{M_6L1_4}\ (PF_6)_{10}]^{2+}$, respectively (Figures S7 and S8). This showed that **1** was a [6 + 4] self-assembly of the ditopic acceptor **M** with the tridentate ligand **L1**. Such a self-assembly can either have an octahedral structure[52] or a double-square shape.[31] Cages with double-square structure are known to have a 1:2 splitting of the ligand peaks,[31] which was not observed in the case of cage **1**. It could thus be concluded that **1** must have an octahedral structure.

The final proof of the structure came from a single-crystal diffraction study (Figures 2 and S9). Crystals suitable for X-ray

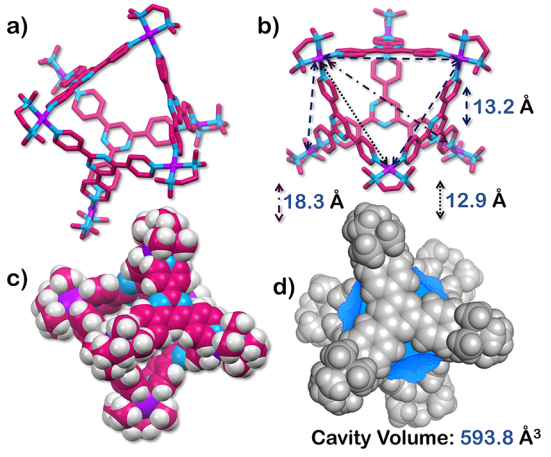

Figure 2. X-ray crystal structure of **1**. (a) Side view of the cage, (b) view of the inner cavity with different Pd−Pd distances labeled, (c) space-fill model of the cage [color scheme: H, white; C, red; N, blue; Pd, violet]. (d) space-fill model with the cavity space highlighted with blue contour.

diffraction were grown by the slow vapor diffusion of acetone into a concentrated aqueous solution of **1** (with NO_3^- as the counterion). A synchrotron radiation source was used for collecting X-ray diffraction data. **1** crystallized in the monoclinic space group $C2/c$ with an octahedral structure. Unlike previously reported octahedral cages,[53] due to the unsymmetrical nature of the ligand **L1**, it did not have a T_d-symmetry. The cage was devoid of any symmetry elements other than a C_2-principal axis. However, the cage crystallized in a centrosymmetric space group with different enantiomers present as one crystal unit making it overall achiral. The crystal structure showed four acceptor (**M**) units, which were present in a nearly square plane, and two acceptor units were positioned above and below the square plane, forming an octahedron. The four ligands (**L1**) were positioned in the alternating faces of this octahedron. The Pd···Pd distance between the two acceptor units above and below the square plane along the C_2-axis is 18.8 Å. The crystal structure also showed that it had a large inner cavity with triangular apertures (Figure 2b). The Pd···Pd distances of the apertures are *ca.* 13.2 Å × 13.2 Å × 12.9 Å. The available volume of the cavity was calculated using the MoloVol software.[54] The cavity volume was found to be 593.8 Å^3 (Figure 2d), which was in the range of that obtained for other octahedral cages.[53]

2.2. Guest Encapsulation Studies. The guest encapsulation of **1** was investigated with electron-rich planar aromatic guests. Excess solid pyrene (**Py**) was added to an aqueous solution of **1**, and the mixture was stirred at room temperature for 8 h. This gave a turbid yellow solution, which was then centrifuged, and the supernatant was used for further characterization. The ^{1}H NMR of this solution (**Py⊂1**) showed new peaks in the region upfield to 7 ppm (Figures 3

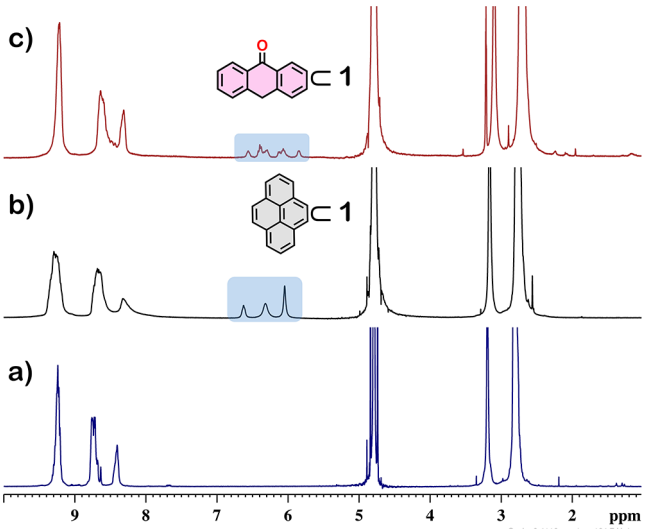

Figure 3. ^{1}H NMR stack plot of (a) **1** in D_2O, (b) **Py⊂1** (**Py**: Pyrene) in D_2O, (c) **AO⊂1** (**AO**: anthrone) in CD_3OD/D_2O (1:2) mixture. The guest peaks are highlighted in blue.

and S10). Similarly, the α-hydrogen peaks of the pyridine rings were shifted downfield (Figures 3 and S10). Such a shift in the ^{1}H NMR peaks of the host and guest molecules was characteristic of guest encapsulation inside the cavity of a cage. The interior binding was further proved by the ^{1}H DOSY spectrum of **Py⊂1** in D_2O, which showed a single diffusion band (log $D = -9.9$) (Figure S13). The host−guest interaction was also confirmed by the ^{1}H−^{1}H NOESY spectrum of **Py⊂1** in D_2O. This showed a correlation between the α-hydrogens of the pyridine rings of **1** and the upfield shifted aromatic protons of **Py** (Figure S14). The host−guest stoichiometry was also calculated by integrating over the host and guest regions and was found to be 1:1 (Figure S12).

Table 1. Reaction Conditions for the Reaction Performed in Molecular Vessels 1 and 2

Entry	Solvent	Atmosphere	Temperature	Light	Time	Cage/Acceptor/Ligand	Major Product	% Composition of the products (P1 + P2) in the $CHCl_3$ extract[a] (Selectivity)[b]
1	Water (H_2O)	Air	r. t.	yes	12 h	Cage 1	**P1**	>99% (99%)
						Cage 2	**P2**	>96% (96%)
2	Water	O_2	r. t.	yes	12 h	Cage 1	**P1**	>99% (99%)
						Cage 2	**P2**	97% (98%)
3	Water	Air	r. t.	yes	2 h	Cage 1	**P1**	>99% (99%)
						Cage 2	**P2**	50% (98%)
4	Water + TEMPO	Air	r. t.	yes	10 h	Cage 1	**NA**[c]	No Reaction
						Cage 2	**P2**	40%[d]
5	Water	Air	r. t.	no	10 h	Cage 1	**P1**	>99% (97%)
						Cage 2	**P2**	95% (99%)
6	Water	Air	<10 °C	no	10 h	Cage 1	**NA**[c]	20%
						Cage 2	**NA**[c]	33%
7	Water	N_2	r. t.	no	10 h	Cage 1	**P1**	>99% (97%)
						Cage 2	**P2**	93% (97%)
8	CH_3CN	N_2	r. t.	no	10 h	Cage 1	**NA**[c]	18%
						Cage 2	**NA**[c]	13%
9	Water	Air	r. t.	yes	10 h	Acceptor **M**	**NA**[c]	<5%
10	Water	Air	r. t.	yes	10 h	Ligand **L1**	**NA**[c]	<5%
						Ligand **L2**	**NA**[c]	23%
11	Water	Air	r. t.	yes	10 h	blank	**NA**[c]	<5%
12	Water+CH_3OH(1:1)	Air	r. t.	yes	10 h	blank	**NA**[c]	<5%

[a]% composition of the products was calculated by ^{1}H NMR, by the relative abundance of the products' (**P1**/**P2**) peaks with respect to that of the starting material (AO) peaks in the $CHCl_3$ extract from the aqueous solution after the reaction. [b]Selectivity was calculated by the relative integration of the **P1** and **P2** peaks. [c]NA denotes that **P1** and/or **P2** are the minor products, and the starting material AO is the major product. [d]Calculated with respect to internal standard as AO peaks were broad due to the presence of TEMPO.

The encapsulation of other polycyclic aromatic hydrocarbons was then investigated using the same procedure as that employed for **Py**. Although **1** showed easy encapsulation of **Py**, it did not show encapsulation of other polyaromatic hydrocarbons except phenanthrene (**P**) (Figures S10 and S14–S16). Interestingly, **1** did not encapsulate the linear isomer anthracene (**A**) but encapsulated the U-shaped isomer phenanthrene (**P**). This is probably due to the shape of the anthracene(**A**) molecule, which failed to have efficient host–guest interactions with **1**. The host–guest interactions were not strong enough to overcome the hydrophobic interactions of **A** with the solvent (H_2O), and thus, the host–guest complex was not formed. Seeing this difference in encapsulation behavior, the encapsulation ability of **1** toward anthracene derivatives was investigated. It was found that **1** readily encapsulated nonplanar derivatives of anthracene like 9,10-dihydroanthracene (Figure S17). It was also able to encapsulate derivatives such as AO [anthracen-9(10*H*)-one] and xanthone [xanthen-9-one] (Figures 3 and S17).

To get an accurate ^{1}H NMR of **AO⊂1**, it was recorded in CD_3OD/D_2O (1:2) mixture by the addition of **AO** (3 equiv in CD_3OD) to a D_2O solution of **1**. It was done in this manner because encapsulation of **AO** (solid) in room temperature for 8 h by **1** led to the formation of other products (*vide infra*, Table 1). Much like the ^{1}H NMR of **Py⊂1**, that of **AO⊂1** also showed new peaks for the guest molecules upfield to the 7 ppm region and a concomitant downfield shift of the host peak. The binding of the guests was further investigated by ^{1}H DOSY NMR of **AO⊂1**. It showed that all the peaks corresponded to the same diffusion band; this proved that the guest and host were part of a single host–guest complex instead of their physical mixture (Figure S18).

2.3. Divergent Synthesis Using Different Cages. Cage **1** showed encapsulation of different guests; thus, its ability to perform chemical reactions within its cavity was investigated. The reaction of choice was the oxidation reaction of 9,10-dihydroanthracene (**H_2A**) or Anthrone (**AO**) to anthraquinone [anthracene-9,10-dione]. This reaction is industrially important as it was used for the commercial production of anthraquinone from coal tar.[55a] Recently, it had been reported that this oxidation can be performed under mild conditions in organic solvents like acetone;[56] however, a report of the reaction in aqueous medium is not known.

The reaction was first investigated with **AO** as the model compound. **AO** possesses an active methylene group (–CH_2–) flanked by two phenyl rings, which could be easily oxidized to a keto group (C═O) leading to the formation of anthraquinone. To an aqueous solution of **1**, solid **AO** (5 mg, excess) was added. The mixture was then stirred in the presence of white light [45 W LED (λ > 400 nm)] in ambient atmosphere and room temperature for 10 h. After this, the mixture was centrifuged, and the clear supernatant was collected. The guest/product encapsulated inside the cage was extracted in chloroform (or $CDCl_3$), which was then characterized by NMR study. The aqueous solution of the cage (after removal of the product) could then be further used for another set of reactions (Scheme S5).

Interestingly, it was found that when the reaction was performed inside cage **1**, a new product (denoted as **P1**) was obtained. **P1** had distinctly different ^{1}H NMR peaks in $CDCl_3$ from that of the starting material **AO** (Figure 4). The reaction proceeded with high selectivity, and only **P1** was formed under the above-mentioned conditions. Needle-shaped yellow crystals of **P1** were easily obtained by the slow evaporation of the chloroform solution. Surprisingly, X-ray analysis of these crystals (Table S2) showed that the compound formed was dianthrone [9,9′-bianthracen-10,10′(9*H*,9′*H*)-dione][55b] in-

stead of expected oxidized product anthraquinone (Figures 4, S29 and S30).

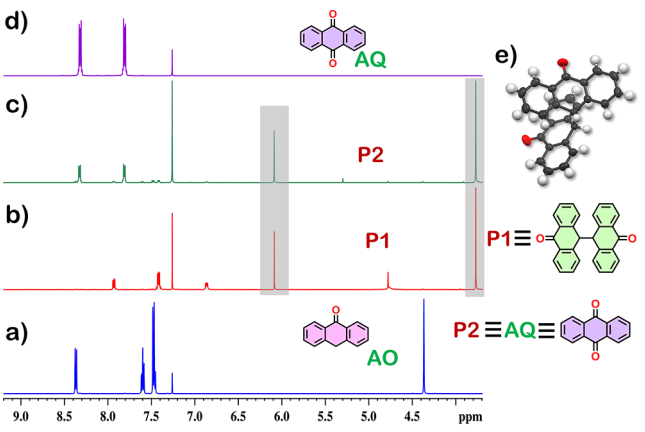

Figure 4. Partial ^{1}H NMR stack plot of (a) Anthrone (**AO**) in $CDCl_3$, (b) product **P1** (in $CDCl_3$) obtained from cage **1**, (c) product **P2** (in $CDCl_3$) obtained from cage **2**, (d) Anthraquinone (**AQ**) in $CDCl_3$, and (e) X-ray crystal structure of **P1** (found to be dianthrone [9,9′-bianthracen-10,10′(9H,9′H)-dione]). Peaks for the internal standard (1,3,5-trimethoxybenzene) are highlighted in gray.

Such unusual dimerization of the active methylene group (sp^3-C) in the confined space of a cage is new. Thus, the uniqueness of this cage toward the formation of such a product was demonstrated. To check this, another water-soluble cage (**2**) with similar $\mathbf{M_6L_4}$ stoichiometry was synthesized (Scheme 1 and S3), following the previously reported procedure from our group.[31] The triimidazole ligand **L2** was self-assembled with the acceptor **M** in a 2:3 molar ratio in water for 24 h at room temperature (Scheme 1 and Figures S19 and S20). This gave a clear solution of **2** that could be further purified by concentrating the solvent and triturating with acetone. The stoichiometry was further verified by the ESI-MS spectrum of the PF_6^- analogue of **2** in acetonitrile. The spectrum showed multiple peaks at m/z = 551.7386, 691.0848, 900.0869, and 1248.4390 corresponding to the fragments $[\mathbf{M_6L2_4}\ (PF_6)_6]^{6+}$, $[\mathbf{M_6L2_4}\ (PF_6)_7]^{5+}$, $[\mathbf{M_6L2_4}\ (PF_6)_8]^{4+}$ and $[\mathbf{M_6L2_4}\ (PF_6)_9]^{3+}$, respectively (Figures S21 and S22).

As seen from the structure of **2** (Figure S23),[31] it has a double-square structure with a D_{2h}-symmetry. Orientation of the ligands in **2** leads to an open structure with two large open windows, like a barrel. **2** also showed encapsulation of multiple planar and nonplanar aromatic molecules (Figures S24–S27). ^{1}H NMR titration of **2** with phenanthrene (**P**) showed that encapsulation of the guest inside **2** showed slow-exchange in ^{1}H NMR time scale (Figures S25 and S26). In such conditions, the peak for the host **2** disappeared, and new peaks for the host–guest species **P⊂2** appeared. In such cases, after a certain equivalence of guest was added, the ^{1}H NMR stopped changing (i.e., no new peak for the host–guest complex appeared), this equivalence directly correlated to the maximum number of guest molecules encapsulated (Figure S25). Using this, the stoichiometry of the host–guest complex was calculated to be 1:1.

Using cage **2**, the same reaction was performed under the same conditions as those for cage **1**. The major product formed using cage **2** (denoted as **P2**) had similar spectral characteristics as that for anthraquinone (**AQ**) (Figures 4, S31 and S32). This observation of formation of different non-isomeric products from the same reaction by simply changing the shape of the reaction vessel (cage) is unusual to the best of our knowledge.

To better understand the reaction of **AO** in reaction vessels **1** and **2**, the reaction was performed under different conditions (Table 1). When the reaction was performed in the presence of [2,2,6,6-tetramethylpiperidin-1-yl)oxyl] (TEMPO), a known radical quencher, in the case of **1**, a negligible amount of **P1** was formed. Similarly, in the case of **2**, the amount of **P2** formed had decreased (Table 1 and Figures S33 and S34). This showed that the reactions inside **1** and **2** occurred through the formation of a radical species, which could be light-mediated or thermally activated. When the reactions in **1** and **2** were performed in absence of light, both reactions showed a very small change in the relative composition of the major product to that obtained in the presence of light (Table 1 and Figures S33 and S34). This meant that even in the absence of light, radical formation could happen. This is probably due to greater stabilization of the radical species inside the cages, which leads to easy formation of the radicals, as has been previously reported.[57] However, when the reaction was performed at low temperature (<10 °C) and in absence of light, the relative composition of the major product decreased significantly, and unreacted **AO** was the major species (Table 1 and Figures S33 and S34). This proved that under such conditions, radical formation was minimized.

It was further seen that the reaction inside cages **1** and **2** occurred even under a N_2 atmosphere (Table 1 and Figures S33 and S34). Formation of **P1** did not depend on any oxidizing species; however, **P2** formation required an oxidizing species. Since the reaction occurred even in a N_2 atmosphere this indicated that the solvent itself was probably acting as a reagent for the formation of **P2**. Similar unusual oxidation by H_2O has been previously reported,[57] where the radical formed inside the cage can react with molecular oxygen or, in its absence, with H_2O to form the oxidized product.

Based on the above findings, **AO** inside cage **1** or **2** readily formed **AO** radical which then dimerized inside cage **1** to form **P1** (dianthrone), while it underwent reaction with molecular oxygen (or in its absence water) inside cage **2** and was oxidized to **P2** (anthraquinone) (Figure S35). The reaction was then investigated in the presence of the subunits **M**, **L1**, and **L2**. While **L1** and **M** showed almost no product formation (<5%), reaction with **L2** showed small conversion but proceeded with the formation of both **P1** and **P2** (Table 1 and Figures S33 and S34). Similarly, when the reaction was performed in absence of any cage or its subcomponents, the reaction hardly proceeded (<5% conversion), and both **P1** and **P2** were formed (Table 1 and Figures S33 and S34). This suggests that the high conversion of **AO** to **P1** or **P2** occurred due to the presence of the cages, and the shape of the cages played an important role in terms of both selectivity and conversion values.

To further check if the divergent reactions inside cages **1** and **2** were due to the change in shape or due to a difference in ligands (**L1** and **L2**), two isomeric cages (**3a** and **3b**) were explored as the reaction vessels (Scheme 2). **3a**[52] has similar octahedral structure as that of **1**, while **3b**[30] has double-square structure as that of **2**. Since **3a** and **3b** were isomeric, change in products could occur due to the change in shape of the cavity and not due to change in the nature of the ligand (Scheme 2).

When the reaction of **AO** was performed inside cage **3a**, product **P1** was selectively formed (Figure S36). However, in this case, the net yield of the dimerized product (**P1**) was less

Scheme 2. Isomeric Pd_6L_4 Cages 3a and 3b Used for the Divergent Synthesis of P1 and P2, Respectively[30,52]

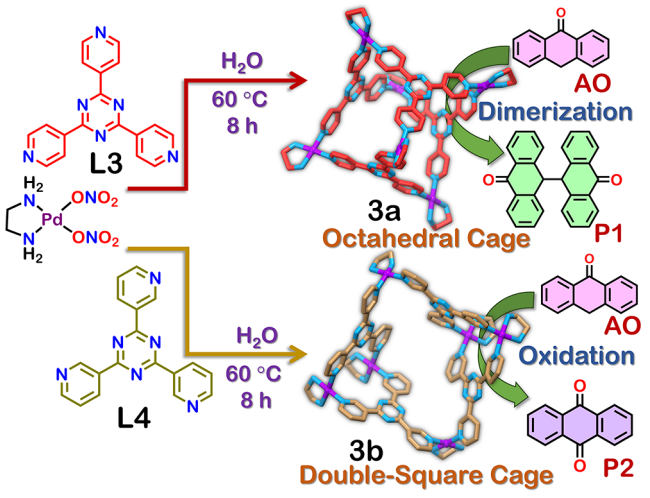

(78%) compared to that using cage **1.** This is attributed to the strong interactions of product **P1** with the host **3a**, and even after stirring the host–guest (**P1⊂3a**) aqueous solution with chloroform for 8 h, all the guest molecules (**P1**) could not be extracted. Reaction of AO inside cage **3b** showed the formation of **P2** as the major product although the selectivity was lower (73%) as compared to that of cage **2** (Figure S36). This indicates that the cavity shape played an important role in the divergent synthesis. To summarize, the aqueous M_6L_4 octahedral cages (**1** and **3a**) preferred the formation of dimerized product (**P1**) from **AO**, while both the double-square shaped aqueous M_6L_4 cages (**2** and **3b**) favored the formation of oxidized anthraquinone (**P2**) from AO under a similar reaction condition.

To check the universality of this reaction, H_2A (9,10-dihydroanthracene) was selected as another guest. To an aqueous solution of **1** or **2**, excess of solid H_2A was added, and the solution was purged with O_2 for 1 min. The mixture was then stirred in the presence of white light [45 W LED (λ > 400 nm)] in room temperature for 10 h. The mixtures were then centrifuged, and clear supernatants were collected. The guests from these solutions were extracted with chloroform, and the ^{1}H NMR spectrum was recorded to analyze the products obtained (Figure S24) using cages **1** and **2** as reaction vessels. The product formation was similar to that observed with **AO**. H_2A inside cage **1** formed **P1**; while in cage **2**, it underwent complete oxidation to form anthraquinone (**P2**) (Figure S37).

2.4. Mechanism of Divergent Synthesis and Selective Encapsulation Studies. Inside cages **1** and **2**, the same compound **AO** was getting transformed to nonisomeric compounds **P1** and **P2**, respectively. For simplicity, the dimerization reaction can be considered as **path-a**, while the oxidation reaction can be considered as **path-b** (Figure S35).

First, the host–guest stoichiometries of **AO⊂1** and **AO⊂2** were investigated. ^{1}H NMR integration of **AO⊂1** in DMSO-d_6/D_2O mixture showed that the stoichiometry was 1:2 (i.e., two molecules of **AO** were encapsulated) (Figure S38). ^{1}H DOSY of the same proved that all the guest molecules were bound to the host (Figure S38). Similarly, ^{1}H NMR titration of **AO⊂2** showed no further change in NMR peaks after the addition of two equivalents of **AO** (Figure S40). Since the titration showed slow-exchange in the ^{1}H NMR time scale (Figure S40), this directly proved that two molecules of **AO** were encapsulated. Then, the relative stabilities of the different host–guest complexes of **1** and **2** with **P1** and **P2** were studied. To check this, a solid mixture of **P1** (9.3 mg, excess) and **P2** (5.0 mg, excess) was added to a concentrated aqueous solution of **1** or **2**. The mixture was then stirred in room temperature for 10 h. The resultant mixture was then centrifuged, and the supernatant was stirred with chloroform to extract the encapsulated guest. It was found that **1** selectively encapsulated **P1** from the mixture of **P1** and **P2**, while cage **2** selectively encapsulated **P2** from the same mixture (Figures 5 and S41–S44).

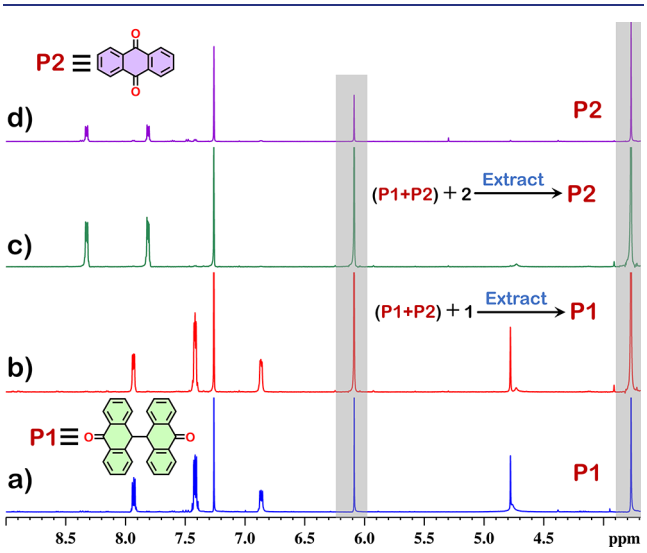

Figure 5. Partial ^{1}H NMR stack plot of (a) **P1**, (b) extracted guest from (**P1** + **P2**) + **1**, (c) extracted guest from (**P1** + **P2**) + **2**, and (d) **P2**. Peaks for the internal standard (1,3,5-trimethoxybenzene) are highlighted in gray.

This was also confirmed by the ^{1}H NMR titration experiments (Figures S46–S52). These clearly showed that **1** only encapsulated **P1** and did not show any encapsulation of **P2** (Figures S46–S48). In case of **2**, **P2** showed complete encapsulation, while in case of **P1,** there was free host peaks remaining (Figures S49–S52). Further, the apparent binding constant[58] of **P1⊂2** (4.86×10^4 M^{-1}) was lower than that of **P2⊂2** (1.08×10^5 M^{-1}). Above results indicate that the formation of **P⊂1** is more favorable than **P2⊂1**. Likewise, **P2⊂2** is more favorable than **P1⊂2**. Using these results, we can predict a mechanism based on selective host–guest chemistry (Figure 6).

AO encapsulated inside **1** underwent a chemical transformation to form **P1⊂1** and **P2⊂1**. **P2⊂1** was not stable (Figure S48), and thus it disintegrated to form free cage **1** and solid **P2**. This free host **1** could then encapsulate any excess of **AO** present in the reaction medium to form **AO⊂1**, which then underwent similar reactions and separation. In this way, after each cycle, the amount of **P1⊂1** increased, and after 10 h, **P1⊂1** remained as the main product in aqueous medium, while **P2** remained as a solid in the precipitate. When the product was extracted using $CHCl_3$ from the aqueous solution, only **P1** was obtained (Figure 4). The presence of **P2** in the precipitate was proved by the ^{1}H NMR of the precipitate (Figure S53). The ^{1}H NMR showed that other than unreacted **AO**, **P2** was the major product in the precipitate. Similarly, **AO**

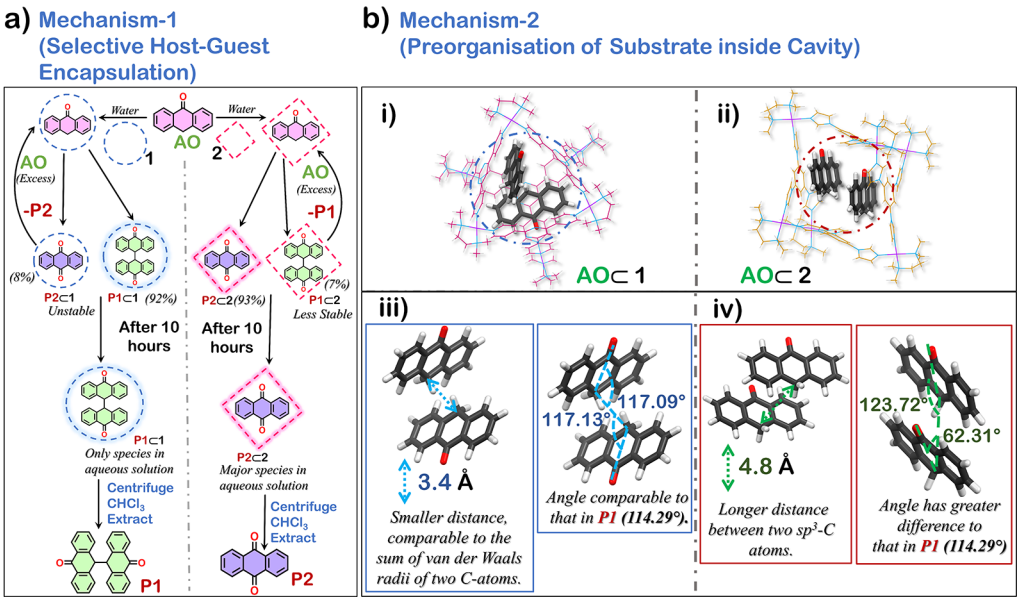

Figure 6. Two probable mechanisms working simultaneously for the selective formation of **P1** in cage **1** and **P2** in cage **2**. (a) Mechanism 1: selective host–guest encapsulation. (b) Mechanism 2: preorganization of substrate inside the cavity [i) optimized structure of **AO⊂1**, (ii) optimized structure of **AO⊂2**, (iii) orientation of **AO** molecules inside cage **1**, and (iv) orientation of **AO** molecules inside cage **2**].

encapsulated inside cage **2** underwent a reaction to form both **P1⊂2** and **P2⊂2**. Because of the lower stability of **P1⊂2**, **P1** came out of the cage, and the free cage (**2**) encapsulated **AO** to form **AO⊂2**, which underwent further cycles of reaction and separation. In this manner, after 10 h in the aqueous solution, **P2⊂2** remained as the major species while more of **P1** remained in the precipitate as solid. When the product was extracted from the aqueous solution, **P2** remained as the major product with 96% selectivity (Figure 4). The ^{1}H NMR of the precipitate proved the presence of more **P1** in the solid phase (Figure S53).

This indicated that the formation of the favorable host–guest complex dictated the flow of the reaction (Figure 6). The reaction with cage **1** proceeds in such a way so as to form the most favorable host–guest complex (**P1⊂1**). Likewise, as **P2⊂2** is the more favorable complex, the reaction with cage **2** proceeded in such a way that the most favorable host–guest complex **P2⊂2** was formed.

This was further verified using **3a** and **3b**. **3b** showed decreased selectivity in the reaction (Figure S36). Thus, **3b** is expected to have a decreased selectivity in host–guest encapsulation. This was observed when encapsulation studies were performed with **3a** and **3b**. While **3a** selectively encapsulated only **P1**, **3b** encapsulated both **P1** and **P2** (Figure S45).

This selective host–guest separation worked only in the presence of excess **AO**. Thus, the relative ratio of **P1** and **P2** formation inside cages **1** and **2** with exactly two equivalents of **AO** (solid) was investigated. The ^{1}H NMR showed that when excess of **AO** was not used, the selectivity for **P1** formation inside **1** went down to 92% from >99% (Figure S55). In the case of cage **2**, the selectivity for **P2** formation went down to 93% from 96% (Figure S56). This indicated that apart from selective-host–guest separation, some other mechanism was also working toward the selective formation of products inside the cages.

To understand the reason behind the inherent tendency of cage **1** to make **P1** and cage **2** to make **P2**, the structure of the host–guest complexes of the substrates (i.e., **AO⊂1** and **AO⊂2**) were optimized semiempirically using the PM6 model (Figure S57). The optimized structures showed that the main stability of the host–guest complexes came from the $\pi-\pi$ interactions of the **AO** molecules with the walls (ligands) of the cages (Figure S57). As cages **1** and **2** differed in their structure (orientation of ligands), the two **AO** molecules encapsulated inside them also had different arrangements (Figure S57).

Interestingly, it was seen that the two **AO** molecules inside cage **1** preorganized in such a manner, that the tetrahedral-C atoms of the two AO molecules were close to one another with 3.4 Å distance (Figures 6 and S58). This distance was comparable to the summation of the van der Waals radii of the two C atoms. This meant that once **AO** radicals were generated inside the cage, they could readily dimerize without needing to overcome a large distance. Further, the angle between the **AO** molecules and an imaginary line connecting the two tetrahedral-C atoms were found to be *ca.* 117°, which was comparable to that observed in **P1** (ca. 114°) (Figures 6 and S58). Thus, if dimerization happened in that arrangement, then the resultant **P1** molecule would not suffer from angle strain (Baeyer strain).

On the other hand, the **AO** molecules inside cage **2** were arranged almost parallel to one another (Figures 6 and S59). The distance (4.8) between the two tetrahedral-C atoms of **AO** was also larger. Thus, two **AO** radicals formed from the **AO** molecules inside cage **2** had less tendency to dimerize. The angle between the two AO molecules and an imaginary line connecting the tetrahedral-C atoms (*ca.* 123 and 62°) also had a larger deviation from the value obtained for **P1** (ca. 114°). Thus, if **AO** molecules dimerized with that arrangement, the resultant **P1** molecule would have high angle strain (Baeyer strain) due to a large deviation of bond angles from the normal values.

The molecules encapsulated inside cages **1** and **2** are confined and show reduced degrees of freedom. Owing to this, such preorganization plays an important role in determining

the selectivity of the reaction taking place inside the cavity. It is due to these reasons that **AO** radicals inside cage **2** preferred to react with the oxygen (or solvent, H_2O) molecule to form **P2** (Figure S35) rather than intermolecular dimerization to form **P1**. While inside cage **1**, the **AO** molecules are preorganized perfectly such that the **AO** radicals could undergo facile dimerization to form **P1**.

The effect of such preorganization toward product formation was previously demonstrated for the Diels–Alder Reaction.[30] The second mechanism (preorganization of the **AO** molecules) seems to be responsible for this divergent chemical transformation inside cages **1** and **2** (Figure 6). This preorganization of the substrate working in conjunction with the selective host–guest separation led to the high selectivity in chemical transformations observed with cages **1** and **2**.

3. CONCLUSIONS

In conclusion, we have demonstrated an unusual example of cage-shape-dependent divergent chemical transformation in an aqueous medium leading to the formation of nonisomeric products. This was done through the synthesis of a new water-soluble M_6L_4 octahedral cage **1**. **1** was obtained in high yield through the metal–ligand-coordination-driven self-assembly of tripyridine ligand **L1** with a *cis*-blocked 90° Pd^{II}-acceptor **M**. The cage has an octahedral structure with a large interior cavity that encapsulated a variety of planar and nonplanar molecules like pyrene and 9,10-dihydroanthracene. Further, it was found that **AO** encapsulated inside **1** was selectively dimerized to dianthrone (**P1**) in aqueous medium when stirred under white light for 10 h at ambient condition. As such a transformation was unusual, the same reaction was performed in a different cage of similar stoichiometry. Under similar conditions, a different M_6L_4 cage (**2**), with double-square shape, caused the oxidation of AO to anthraquinone (**P2**) inside its cavity. This dichotomy in the reaction pathway by changing the molecular shape of the reaction vessel is a new observation. The role of cavity shape on the fate of same chemical reaction was further investigated using other cages like **3a** and **3b** that are isostructural to **1** and **2**, respectively. It was found that isostructural M_6L_4 cages (**1** and **3a**) with an octahedral shape preferred the formation of **P1** inside their cavity. Similarly, the aqueous M_6L_4 cages (**2** and **3b**) with double-square structure favored the formation of **P2** inside their cavity. Selective encapsulation studies showed that in cage **1**, **P1⊂1** was the more favorable host–guest complex, and **P2⊂2** was the more favorable host–guest complex in cage **2**. This showed a unique correlation between product formation and favorable host–guest complexation. Optimization of the structures of the host–guest complexes, **AO⊂1** and **AO⊂2**, showed that the **AO** molecules were preorganized inside cage **1** in such a manner that it facilitated the dimerization reaction to form **P1**. The absence of such favorable preorganization inside cage **2** led to a different reaction pathway, where **AO** reacted with oxygen (or the solvent H_2O) to form **P2**. Through this, we demonstrated a new form of divergent chemical transformation, where the nature of the cavity and its host–guest interactions (substrate preorganization and host–guest binding preference) dictated the nature of the final product and reaction pathways. We envision that this divergent synthesis strategy can be used further in other macromolecular hosts leading to the formation of more diverse molecules.

■ ASSOCIATED CONTENT

Supporting Information

The Supporting Information is available free of charge at https://pubs.acs.org/doi/10.1021/jacs.3c10191.

Additional NMR, ESI-MS spectra, experimental details, and optimized structures; X-ray crystallographic data for **1**; and X-ray crystallographic data for **P1** (PDF)

Accession Codes

CCDC 2281646 contains the supplementary crystallographic data for this paper. These data can be obtained free of charge via www.ccdc.cam.ac.uk/data_request/cif, or by emailing data_request@ccdc.cam.ac.uk, or by contacting The Cambridge Crystallographic Data Centre, 12 Union Road, Cambridge CB2 1EZ, UK; fax: +44 1223 336033.

■ AUTHOR INFORMATION

Corresponding Author

Partha Sarathi Mukherjee − *Department of Inorganic and Physical Chemistry, Indian Institute of Science, Bangalore 560012, India;* orcid.org/0000-0001-6891-6697; Email: psm@iisc.ac.in

Authors

Debsena Chakraborty − *Department of Inorganic and Physical Chemistry, Indian Institute of Science, Bangalore 560012, India;* orcid.org/0000-0003-0354-9085

Shamsad Ali − *Department of Inorganic and Physical Chemistry, Indian Institute of Science, Bangalore 560012, India*

Pritam Choudhury − *Department of Inorganic and Physical Chemistry, Indian Institute of Science, Bangalore 560012, India*

Neal Hickey − *Department of Chemical and Pharmaceutical Sciences, University of Trieste, Trieste 34127, Italy;* orcid.org/0000-0003-1271-5719

Complete contact information is available at: https://pubs.acs.org/10.1021/jacs.3c10191

Notes

The authors declare no competing financial interest.

■ ACKNOWLEDGMENTS

P.S.M. thanks the SERB (New Delhi) for research grant (CRG-2022/000494) and DST-FIST for NMR facility. D.C. and S.A. gratefully acknowledge PMRF (India) for research fellowship. Authors are grateful to Dr. Garima Jindal for fruitful discussion/suggestions on the mechanism of the reaction during the revision of this paper.

■ REFERENCES

(1) Weckhuysen, B. M.; Kitagawa, S.; Tsapatsis, M. Reactions in Confined Spaces. *ChemPhysChem* **2018**, *19*, 339–340.

(2) Gao, J.; Ma, S.; Major, D. T.; Nam, K.; Pu, J.; Truhlar, D. G. Mechanisms and Free Energies of Enzymatic Reactions. *Chem. Rev.* **2006**, *106*, 3188–3209.

(3) Yang, Z.; Esteve, F.; Antheaume, C.; Lehn, J.-M. Dynamic Covalent Self-Assembly And Self-Sorting Processes In The Formation Of Imine-Based Macrocycles And Macrobicyclic Cages. *Chem. Sci.* **2023**, *14*, 6631–6642.

(4) Gupta, G.; Sun, Y.; Das, A.; Stang, P. J.; Yeon Lee, C. BODIPY Based Metal-Organic Macrocycles And Frameworks: Recent Therapeutic Developments. *Coord. Chem. Rev.* **2022**, *452*, 214308.

(5) Zenka, M.; Preinl, J.; Pertermann, E.; Lützen, A.; Tiefenbacher, K. A Water- and Base-Stable Iminopyridine-Based Cage That Can Bind Larger Organic Anions. *Eur. J. Inorg. Chem.* **2023**, *26*, No. e202300110.
(6) Lin, X.; Chen, F.; Yu, X.; Wang, H.; Qiu, H.; Li, Y.; Yin, S.; Stang, P. J. Phenylthiol-BODIPY-Based Supramolecular Metallacycles For Synergistic Tumor Chemo-Photodynamic Therapy. *Proc. Natl. Acad. Sci. U.S.A.* **2022**, *119*, No. e2203994119.
(7) Zhu, H.; Liu, J.; Wu, Y.; Wang, L.; Zhang, H.; Li, Q.; Wang, H.; Xing, H.; Sessler, J. L.; Huang, F. Substrate-Responsive Pillar[5]arene-Based Organic Room-Temperature Phosphorescence. *J. Am. Chem. Soc.* **2023**, *145*, 11130−11139.
(8) Lin, H.-Y.; Zhou, L.-Y.; Mei, F.; Dou, W.-T.; Hu, L.; Yang, H.-B.; Xu, L. Highly Efficient Self-Assembly of Metallacages and Their Supramolecular Catalysis Behaviors in Microdroplets. *Angew. Chem., Int. Ed.* **2023**, *62*, No. e202301900.
(9) Tromans, R. A.; Carter, T. S.; Chabanne, L.; Crump, M. P.; Li, H.; Matlock, J. V.; Orchard, M. G.; Davis, A. P. A Biomimetic Receptor For Glucose. *Nat. Chem.* **2019**, *11*, 52−56.
(10) Chakraborty, D.; Modak, R.; Howlader, P.; Mukherjee, P. S. De Novo Approach For The Synthesis Of Water-Soluble Interlocked And Non-Interlocked Organic Cages. *Chem. Commun.* **2021**, *57*, 3995−3998.
(11) Li, X.; Lin, W.; Sharma, V.; Gorecki, R.; Ghosh, M.; Moosa, B. A.; Aristizabal, S.; Hong, S.; Khashab, N. M.; Nunes, S. P. Polycage Membranes For Precise Molecular Separation And Catalysis. *Nat. Commun.* **2023**, *14*, 3112.
(12) Sun, S.; Liu, M.; Thapa, J.; Hartono, N. T. P.; Zhao, Y.; He, D.; Wieghold, S.; Chua, M.; Wu, Y.; Bulović, V.; Ling, S.; Brabec, C. J.; Cooper, A. I.; Buonassisi, T. Cage Molecules Stabilize Lead Halide Perovskite Thin Films. *Chem. Mater.* **2022**, *34*, 9384−9391.
(13) Xu, Q.; Wang, X.; Huang, S.; Hu, Y.; Teat, S. J.; Settineri, N. S.; Chen, H.; Wayment, L. J.; Jin, Y.; Sharma, S.; Zhang, W. Dynamic Covalent Self-sorting in Molecular and Polymeric Architectures Enabled by Spiroborate Bond Exchange. *Angew. Chem., Int. Ed.* **2023**, *62*, No. e202304279.
(14) Samanta, J.; Natarajan, R. Cofacial Organic Click Cage to Intercalate Polycyclic Aromatic Hydrocarbons. *Org. Lett.* **2016**, *18*, 3394−3397.
(15) Percástegui, E. G.; Mosquera, J.; Ronson, T. K.; Plajer, A. J.; Kieffer, M.; Nitschke, J. R. Waterproof Architectures Through Subcomponent Self-Assembly. *Chem. Sci.* **2019**, *10*, 2006−2018.
(16) Liu, S.-Y.; Kishida, N.; Kim, J.; Fukui, N.; Haruki, R.; Niwa, Y.; Kumai, R.; Kim, D.; Yoshizawa, M.; Shinokubo, H. Realization of Stacked-Ring Aromaticity in a Water-Soluble Micellar Capsule. *J. Am. Chem. Soc.* **2023**, *145*, 2135−2141.
(17) Konopka, M.; Cecot, P.; Harrowfield, J. M.; Stefankiewicz, A. R. Structural Self-Sorting Of Pseudopeptide Homo And Heterodimeric Disulfide Cages In Water: Mechanistic Insights And Cation Sensing. *J. Mater. Chem. C* **2021**, *9*, 7607−7614.
(18) Caprice, K.; Pál, D.; Besnard, C.; Galmés, B.; Frontera, A.; Cougnon, F. B. L. Diastereoselective Amplification of a Mechanically Chiral [2]Catenane. *J. Am. Chem. Soc.* **2021**, *143*, 11957−11962.
(19) Tay, H. M.; Beer, P. Optical Sensing Of Anions By Macrocyclic And Interlocked Hosts. *Org. Biomol. Chem.* **2021**, *19*, 4652−4677.
(20) Benavides, P. A.; Gordillo, M. A.; Yadav, A.; Joaqui-Joaqui, M. A.; Saha, S. Pt(Ii)-Coordinated Tricomponent Self-Assemblies Of Tetrapyridyl Porphyrin And Dicarboxylate Ligands: Are They 3D Prisms Or 2D Bow-Ties? *Chem. Sci.* **2022**, *13*, 4070−4081.
(21) Orton, G. R. F.; Pilgrim, B. S.; Champness, N. R. The Chemistry Of Phosphines In Constrained, Well-Defined Micro-environments. *Chem. Soc. Rev.* **2021**, *50*, 4411−4431.
(22) Samanta, D.; Galaktionova, D.; Gemen, J.; Shimon, L. J. W.; Diskin-Posner, Y.; Avram, L.; Král, P.; Klajn, R. Reversible Chromism Of Spiropyran In The Cavity Of A Flexible Coordination Cage. *Nat. Commun.* **2018**, *9*, 641.
(23) Chakraborty, D.; Saha, R.; Clegg, J. K.; Mukherjee, P. S. Selective Separation Of Planar And Non-Planar Hydrocarbons Using An Aqueous Pd6 Interlocked Cage. *Chem. Sci.* **2022**, *13*, 11764−11771.
(24) Yuasa, M.; Sumida, R.; Tanaka, Y.; Yoshizawa, M. Selective Encapsulation and Unusual Stabilization of cis-Isomers by a Spherical Polyaromatic Cavity. *Chem.-—Eur. J.* **2022**, *28*, No. e202104101.
(25) Zhang, Z.; Zhao, Z.; Hou, Y.; Wang, H.; Li, X.; He, G.; Zhang, M. Aqueous Platinum(II)-Cage-Based Light-Harvesting System for Photocatalytic Cross-Coupling Hydrogen Evolution Reaction. *Angew. Chem., Int. Ed.* **2019**, *58*, 8862−8866.
(26) Jia, P.-P.; Hu, Y.-X.; Peng, Z.-Y.; Song, B.; Zeng, Z.-Y.; Ling, Q.-H.; Zhao, X.; Xu, L.; Yang, H.-B. Construction of an Artificial Light-Harvesting System with Efficient Photocatalytic Activity in an Aqueous Solution Based on a FRET-Featuring Metallacage. *Inorg. Chem.* **2023**, *62*, 1950−1957.
(27) Acharyya, K.; Bhattacharyya, S.; Lu, S.; Sun, Y.; Mukherjee, P. S.; Stang, P. J. Emissive Platinum(II) Macrocycles as Tunable Cascade Energy Transfer Scaffolds. *Angew. Chem., Int. Ed.* **2022**, *61*, No. e202200715.
(28) Percástegui, E. G.; Ronson, T. K.; Nitschke, J. R. Design and Applications of Water-Soluble Coordination Cages. *Chem. Rev.* **2020**, *120*, 13480−13544.
(29) Banerjee, R.; Chakraborty, D.; Mukherjee, P. S. Molecular Barrels as Potential Hosts: From Synthesis to Applications. *J. Am. Chem. Soc.* **2023**, *145*, 7692−7711.
(30) (a) Yoshizawa, M.; Tamura, M.; Fujita, M. Diels-Alder in Aqueous Molecular Hosts: Unusual Regioselectivity and Efficient Catalysis. *Science* **2006**, *312*, 251−254. (b) Bar, A. K.; Chakrabarty, R.; Mukherjee, P. S. Self-Assembly of a Pd_6-Molecular Double-Square and a Cu_3-Trigonalbipyramidal Cage via a New Tripodal Flexible Ligand. *Inorg. Chem.* **2009**, *48*, 10880−10882.
(31) Samanta, D.; Mukherjee, S.; Patil, Y. P.; Mukherjee, P. S. Self-Assembled Pd6 Open Cage with Triimidazole Walls and the Use of Its Confined Nanospace for Catalytic Knoevenagel- and Diels-Alder Reactions in Aqueous Medium. *Chem.-—Eur. J.* **2012**, *18*, 12322−12329.
(32) Nguyen, Q. N. N.; Xia, K. T.; Zhang, Y.; Chen, N.; Morimoto, M.; Pei, X.; Ha, Y.; Guo, J.; Yang, W.; Wang, L.-P.; Bergman, R. G.; Raymond, K. N.; Toste, F. D.; Tantillo, D. J. Source of Rate Acceleration for Carbocation Cyclization in Biomimetic Supramolecular Cages. *J. Am. Chem. Soc.* **2022**, *144*, 11413−11424.
(33) Bierschenk, S. M.; Pan, J. Y.; Settineri, N. S.; Warzok, U.; Bergman, R. G.; Raymond, K. N.; Toste, F. D. Impact of Host Flexibility on Selectivity in a Supramolecular Host-Catalyzed Enantioselective aza-Darzens Reaction. *J. Am. Chem. Soc.* **2022**, *144*, 11425−11433.
(34) Crawley, M. R.; Zhang, D.; Cook, T. R. Electrocatalytic Production Of Hydrogen Peroxide Enabled By Post-Synthetic Modification Of A Self-Assembled Porphyrin Cube. *Inorg. Chem. Front.* **2023**, *10*, 316−324.
(35) Cai, L.-X.; Li, S.-C.; Yan, D.-N.; Zhou, L.-P.; Guo, F.; Sun, Q.-F. Water-Soluble Redox-Active Cage Hosting Polyoxometalates for Selective Desulfurization Catalysis. *J. Am. Chem. Soc.* **2018**, *140*, 4869−4876.
(36) Banerjee, R.; Chakraborty, D.; Jhang, W.-T.; Chan, Y.-T.; Mukherjee, P. S. Structural Switching of a Distorted Trigonal Metal-Organic Cage to a Tetragonal Cage and Singlet Oxygen Mediated Oxidations. *Angew. Chem., Int. Ed.* **2023**, *62*, No. e202305338.
(37) Pullen, S.; Löffler, S.; Platzek, A.; Holstein, J. J.; Clever, G. H. Substrate And Product Binding Inside A Stimuli-Responsive Coordination Cage Acting As A Singlet Oxygen Photosensitizer. *Dalton Trans.* **2020**, *49*, 9404−9410.
(38) Bobylev, E. O.; Poole, D. A., III; de Bruin, B.; Reek, J. N. H. M6L12 Nanospheres with Multiple C70 Binding Sites for 1O2 Formation in Organic and Aqueous Media. *J. Am. Chem. Soc.* **2022**, *144*, 15633−15642.
(39) Ngai, C.; Wu, H.-T.; da Camara, B.; Williams, C. G.; Mueller, L. J.; Julian, R. R.; Hooley, R. J. Moderated Basicity of Endohedral Amine Groups in an Octa-Cationic Self-Assembled Cage. *Angew. Chem., Int. Ed.* **2022**, *61*, No. e202117011.

(40) Martí-Centelles, V.; Lawrence, A. L.; Lusby, P. J. High Activity and Efficient Turnover by a Simple, Self-Assembled "Artificial Diels-Alderase. *J. Am. Chem. Soc.* **2018**, *140*, 2862−2868.
(41) Hong, T.; Zhang, Z.; Sun, Y.; Tao, J.-J.; Tang, J.-D.; Xie, C.; Wang, M.; Chen, F.; Xie, S.-S.; Li, S.; Stang, P. J. Chiral Metallacycles as Catalysts for Asymmetric Conjugate Addition of Styrylboronic Acids to α,β-Enones. *J. Am. Chem. Soc.* **2020**, *142*, 10244−10249.
(42) Das, A.; Mandal, I.; Venkatramani, R.; Dasgupta, J. Ultrafast Photoactivation Of C-H Bonds Inside Water-Soluble Nanocages. *Sci. Adv.* **2019**, *5*, No. eaav4806.
(43) Kang, J.; Rebek, J. Acceleration Of A Diels-Alder Reaction By A Self-Assembled Molecular Capsule. *Nature* **1997**, *385*, 50−52.
(44) Salles, A. G., Jr.; Zarra, S.; Turner, R. M.; Nitschke, J. R. A Self-Organizing Chemical Assembly Line. *J. Am. Chem. Soc.* **2013**, *135*, 19143−19146.
(45) Zhu, F.-F.; Chen, L.-J.; Chen, S.; Wu, G.-Y.; Jiang, W.-L.; Shen, J.-C.; Qin, Y.; Xu, L.; Yang, H.-B. Confinement Self-Assembly of Metal-Organic Cages within Mesoporous Carbon for One-Pot Sequential Reactions. *Chem* **2020**, *6*, 2395−2406.
(46) Takezawa, H.; Fujii, Y.; Murase, T.; Fujita, M. Electrophilic Spirocyclization of a 2-Biphenylacetylene via Conformational Fixing within a Hollow-Cage Host. *Angew. Chem., Int. Ed.* **2022**, *61*, No. e202203970.
(47) Burke, M. D.; Schreiber, S. L. A Planning Strategy for Diversity-Oriented Synthesis. *Angew. Chem., Int. Ed.* **2004**, *43*, 46−58.
(48) Lee, Y.-C.; Kumar, K.; Waldmann, H. Ligand-Directed Divergent Synthesis of Carbo- and Heterocyclic Ring Systems. *Angew. Chem., Int. Ed.* **2018**, *57*, 5212−5226.
(49) Li, J.; Luo, Y.; Cheo, H. W.; Lan, Y.; Wu, J. Photoredox-Catalysis-Modulated, Nickel-Catalyzed Divergent Difunctionalization of Ethylene. *Chem* **2019**, *5*, 192−203.
(50) Grommet, A. B.; Lee, L. M.; Klajn, R. Molecular Photoswitching in Confined Spaces. *Acc. Chem. Res.* **2020**, *53*, 2600−2610.
(51) Brown, C. J.; Toste, F. D.; Bergman, R. G.; Raymond, K. N. Supramolecular Catalysis in Metal-Ligand Cluster Hosts. *Chem. Rev.* **2015**, *115*, 3012−3035.
(52) Murase, T.; Nishijima, Y.; Fujita, M. Cage-Catalyzed Knoevenagel Condensation under Neutral Conditions in Water. *J. Am. Chem. Soc.* **2012**, *134*, 162−164.
(53) Liu, H.-K.; Ronson, T. K.; Wu, K.; Luo, D.; Nitschke, J. R. Anionic Templates Drive Conversion between a ZnII9L6 Tricapped Trigonal Prism and ZnII6L4 Pseudo-Octahedra. *J. Am. Chem. Soc.* **2023**, *145*, 15990−15996.
(54) Maglic, J. B.; Lavendomme, R. Molovol: An Easy-To-Use Program For Analyzing Cavities, Volumes And Surface Areas Of Chemical Structures. *J. Appl. Crystallogr.* **2022**, *55*, 1033−1044.
(55) (a) Bennett, C. B.; Sherman, D. R. Crude Anthracene Separation. US Patent 2,438,148 A, 1945. (b) Chang, M.-Y.; Tsai, C.-Y.; Chan, C.-K. mCPBA-Mediated Conjugation Of Dibenzosuberenone And Amines Or Carboxylic Acids. *Tetrahedron* **2015**, *71*, 424−430.
(56) Jiang, D.; Hu, W.; Chen, M.; Fu, Z.; Su, A.; Yang, B.; Mao, F.; Zhang, C.; Liu, Y.; Yin, D. Visible-Light-Triggered Quantitative Oxidation of 9,10-Dihydroanthracene to Anthraquinone by O2 under Mild Conditions. *ChemSusChem* **2020**, *13*, 1785−1792.
(57) Yoshizawa, M.; Miyagi, S.; Kawano, M.; Ishiguro, K.; Fujita, M. Alkane Oxidation via Photochemical Excitation of a Self-Assembled Molecular Cage. *J. Am. Chem. Soc.* **2004**, *126*, 9172−9173.
(58) Yang, D.; Greenfield, J. L.; Ronson, T. K.; von Krbek, L. K. S.; Yu, L.; Nitschke, J. R. LaIII and ZnII Cooperatively Template a Metal-Organic Capsule. *J. Am. Chem. Soc.* **2020**, *142*, 19856−19861.